

Initial Results of Ichon Solar Radio Spectrograph

K. -S. CHO^{1,2}, K. -S. KIM², Y. -J. MOON^{3,4} and M. DRYER^{5,6}

¹ *Radio Research Laboratory, Ichon, Kyunggi-do, 467-880, Republic of Korea*
(kscho@rrl.go.kr)

² *Department of Astronomy and Space Science, Kyunghee University, Yongin, Kyunggi-do, 449-701, Republic of Korea* (kskim@khu.ac.kr)

³ *Big Bear Solar Observatory/NJIT, 40386 North Shore Lane, Big Bear City, CA 92314, U.S.A.* (yjmoon@bbso.njit.edu)

⁴ *Korea Astronomy Observatory, Daejeon 305-348, Republic of Korea*

⁵ *Space Environment Center, National Oceanic and Atmospheric Administration, Boulder, CO 80303-3328, U.S.A.* (murray.dryer@noaa.gov)

⁶ *Geophysical Institute, University of Alaska, Fairbanks, AK 99775-7320, U.S.A.*

(Received 1 April 2002 ; Accepted 10 September 2002)

Abstract. A new solar radio spectrograph to observe solar radio bursts has been installed at Ichon branch of Radio Research Laboratory, Ministry of Information and Communication, Korea. The spectrograph consists of three different antennas to sweep a wide band of frequencies in the range of 30 MHz \sim 2500 MHz. Its daily operation is fully automated and typical examples of solar radio bursts have been successfully observed. In this paper we describe briefly its hardware and data processing methods. Then we present coronal shock speeds estimated for 34 type II bursts from May 1998 to November 2000 and compare them with those from other observatories. We also present the close relationship between onset time of Type II bursts and X-ray flares as well as their associations with coronal mass ejections.

1. Introduction

Solar radio bursts are non-thermal emission and represent dynamic processes occurring in the corona. Wild and McCready (1950) classified solar radio bursts into five major types. The bursts are started at frequencies as high as 500 MHz (Vrsnak *et al.*, 1995) down to the ionospheric cut off (\sim 15 MHz). A number of ground-based broadband radio spectrographs have been developed and used for the observation of solar radio bursts in the centimeter to decameter wavelengths (e.g., Mann *et al.*, 1992; Prestage *et al.*, 1994; Kondo *et al.*, 1995; Messmer *et al.*, 1999; Shanmugaraju *et al.*, 1999).

Type II radio bursts appear as emission stripes slowly drifting from high to low frequencies in the dynamic spectrogram. Using statistical analysis of the type II burst, Mann *et al.* (1996) found that a drift rate of the type II bursts is -0.16 ± 0.11 MHz s⁻¹ and the life time of the type II burst is in the range 5 to 15 min. Type II bursts are thought to be generated by Langmuir turbulence due to accelerated electrons at the shock (see, e.g., Krüger, 1979). As a shock propagates



© 2002 Kluwer Academic Publishers. Printed in the Netherlands.

away from the Sun, the density of ambient electrons decreases and so does the excited frequency ($f \simeq f_p$), as may be seen on a dynamic spectrogram. Thus the drift rate can be converted into the shock speed by employing an appropriate coronal electron density model (Smerd *et al.*, 1975; Robinson *et al.*, 1985).

There has been the long-standing controversy about the relationship among metric type II bursts, flares and CMEs (Wagner and McQueen, 1983; Gosling, 1993; Gosling and Hundhausen, 1995; Svestka, 1995; Dryer, 1996; Gopalswamy *et al.*, 1998; Cliver *et al.*, 1999). Gopalswamy *et al.* (1998) proposed that metric type II bursts are produced by flares and then supported the idea that the metric type II shocks (coronal shocks) and deka-hectometric (D-H) type II shocks (interplanetary shocks) are of independent origin (Wagner and McQueen, 1983). On the other hand, Cliver *et al.* (1999) insisted that metric type II, EIT wave, and D-H type II bursts are driven by fast CMEs. The recent observed EIT waves are found to be associated with metric type II bursts (Klassen *et al.*, 2000; Gopalswamy *et al.*, 2000) in their speeds and positions as well as with CMEs (Thompson *et al.*, 2000). Recently, Reiner *et al.* (2001) found no obvious correlation between shock parameters derived from metric type II radio bursts and the corresponding CME speeds. Leblanc *et al.* (2001) also showed from 10 type II bursts that the CME lift-offs took place before the flares and type II bursts by 1-24min for most of the selected events using the extrapolation of the CME liftoff time and its speed in the radial direction above the active region. However, in some events, they noted that the CME liftoff, type II initiation and progressions are essentially simultaneous. Thus, they argued that the shock waves may be driven by the CMEs all the way from $\sim 1R_s$ to 1 AU. In addition, they admitted for some events that the evidence available cannot exclude the hypothesis that the shock is a blast wave from the flare to 1 AU (Smart and Shea, 1985). Due to the complex relationship between type II emitting shocks and the associated CMEs or flares, the controversy is not yet resolved.

Type II coronal shock speeds have been largely employed by real-time shock prediction models such as the Interplanetary Shock Propagation Model (ISPM) (based on a parametric 2 - 1/2D MHD study by Smith and Dryer, 1990) and the Shock Time of Arrival Model (STOA) (Dryer and Smart, 1984; Smart and Shea, 1985). These models predict the time of arrival and strength of solar-initiated interplanetary shocks at 1 AU. Since the shock arrival time at the Earth implies the starting of geomagnetic disturbances by combining with the possibilities of southern components of interplanetary magnetic field (for review, Dryer, 1994), type II burst data have been regarded to be quite significant in solar-terrestrial connection studies. Coronal shock velocities obtained

from type II burst data were used as one of the basic inputs data for the models.

Thompson *et al.* (1996) compared the shock speeds derived from radio bursts observed by the Swept Frequency Interferometric Radiometer (SFIR) equipment at the US Air Force Radio Solar Telescope Network (USAF/RSTN) with those derived from the Culgoora radio spectrograph. The Culgoora frequency bandwidth extended from 18 to 1800 MHz, whereas the older USAF/RSTN bandwidth covered only 25 to 85 MHz with analog output. The latter sites have recently been upgraded in frequency to a bandwidth from 25 to 180 MHz using digital techniques. They showed that the RSTN shock speeds were 1.5 - 3.0 times larger than the Culgoora values. This difference is mainly attributed to the smaller frequency bandwidth of the SFIR instruments wherein it was often difficult to distinguish between the fundamental and harmonic bursts, the former sometimes being absorbed by the ionosphere. Thus, the harmonic was easily (especially with interference from the interferometer) mistaken and taken to be the fundamental. These results imply that a wide bandwidth coverage is important for accurate estimation of coronal shock speeds.

In this paper we introduce a new solar radio spectrograph recently installed at Ichon branch of Radio Research Laboratory, Korea. This paper briefly describes the new spectrograph and presents initial results of coronal shock speeds estimated from 34 type II burst data which were observed from May 1998 to November 2000. We also examine the relationship between onset time of our type II bursts and X-ray starts/peaks as well as their association with CMEs. An early progress report on hardware and software details, written in the Korean language, was given by Cho *et al.* (1997).

We describe the Ichon hardware and data analysis procedures in Section 2, the results in Section 3, and a summary and discussion on our results in Section 4.

2. Hardware and Data Analysis

The new radio spectrograph has been operated for monitoring the solar radio emission in the range between 30 up to 2500 MHz at the Ichon ($N37.15^\circ$, $E127.55^\circ$) branch of Radio Research Laboratory since May, 1998. The system is composed of three different frequency band antennas, which are pointed continuously at the Sun throughout the daytime. First one (Ichon Radio Spectrograph: IRS-1) is a spatially crossed 15-element LPA (log-periodic antenna) in the 30 - 100 MHz band; the second (IRS-2) is a 10 m parabolic dish with a crossed 20-element LPA

Table I. Major Characteristics of Ichon Radio Spectrograph(IRS)

Parameter	IRS-1	IRS-2	IRS-3
Antenna gain (dBi)	10.33	17.5 (100 MHz) 31.4 (500 MHz)	27.0 (500 MHz) 40.8 (2500 MHz)
Channel bandwidth	0.14 MHz	0.71 MHz	2.85 MHz
Beam width	60°	20° (100 MHz) 4.1° (500 MHz)	6.8° (500 MHz) 1.4° (2500 MHz)
LNA ^a (dB)	45 (gain) 1.3 (noise figure)	45 (gain) 1.6 (noise figure)	32 (gain) 2.0 (noise figure)
BPF ^b	30-100 MHz	100-500 MHz (325 MHz Notch)	500-2500 MHz
Polarization	RHCP ^c /LHCP ^d	RHCP/LHCP	RHCP/LHCP

^a Low Noise Amplifier.

^b Band Pass Filter.

^c Right Hand Circular Polarization.

^d Left Hand Circular Polarization.

in the 100 - 500 MHz band; and the third (IRS-3) is a 6m parabolic dish with a crossed 23-element LPA in the 500 - 2500 MHz range. To derive the circular polarized components, linear components from a crossed LPA are combined with a 90-hybrid combiner, which works over a wide frequency range. Band pass filters for each of the bands and notch filters with rejection frequency (centered on 325 MHz) are placed between the hybrid combiner and LNA (Low Noise Amplifier) to prevent saturation of amplifier by strong signals. Major characteristics of the hardware subsystem are summarized in Table I. Some parts of the system are similar to those of the Hiraiso radio spectrograph (Kondo *et al.*, 1995).

Daily observation is performed nearly automatically from data acquisition to processing. PC (Personal Computer) performs data acquisition from six spectrum analyzers of full frequency range at every three seconds via the GPIB (General Purpose Interface Bus). Acquired data are immediately transferred to a workstation through the LAN (Local Area Network) and are then stored on a hard disk. The time resolution is about 3 seconds, which implies the total time for gathering a set of data with all frequencies. For other applications, the time resolution can be changed. Data processing includes the elimination of artificial noises and the subtraction of solar background

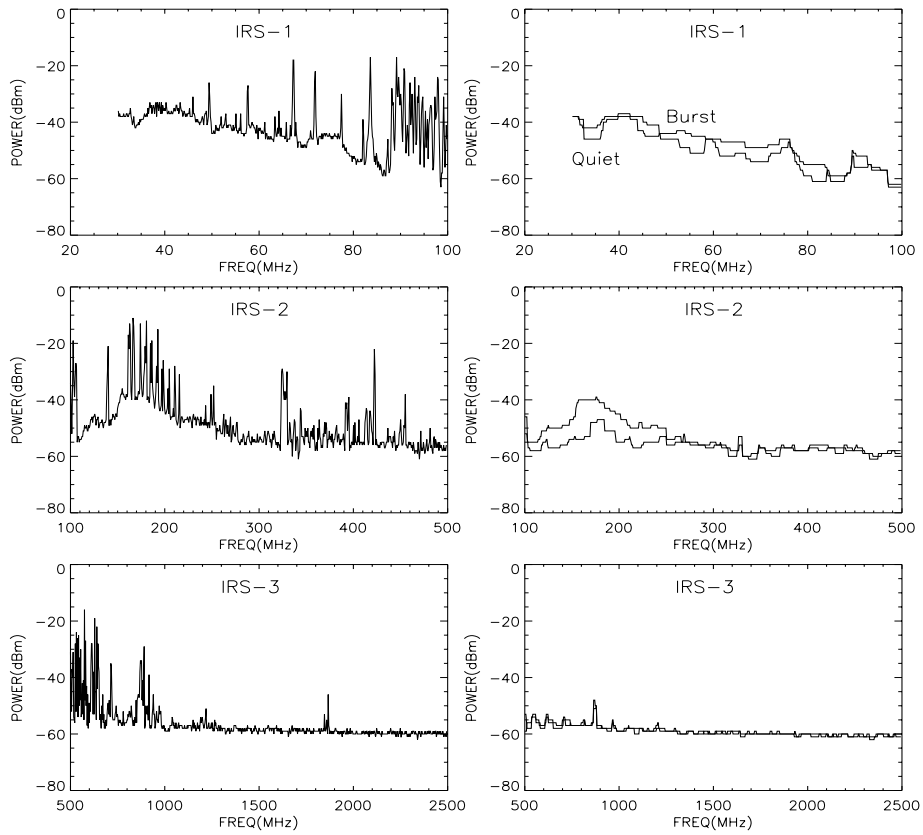


Figure 1. Raw spectra (left panels) detected by IRS for three bands and the re-sampled spectra of quiet and burst emission (thin solid line) by the minimum smoothing method.

emissions to improve the quality of the solar burst spectrogram. At every hour, our near real-time spectrograph image is updated on the web (http://solaradio.rrl.go.kr/ie/realddata/rrl_sun.htm) after the data processing. We have devised a minimum smoothing method, a part of post-analysis, which selects a minimum value for a given frequency window: 2 MHz (30 ~ 100 MHz), 8 MHz (100 ~ 500 MHz), and 20 MHz (500 ~ 2500 MHz). The adopted window sizes were determined from several trials and are mainly used for the estimation of drift rates. They can be changed for other applications. Left panels of Figure 1 show the raw spectra for all observation bands and right panels are re-sampled spectra of quiet and burst emissions after applying the minimum smoothing method. As shown in the figures, most interferences are effectively removed by the minimum smoothing method, and the radio bursts are also clearly discernible from background emission. To

separate burst events in the dynamic spectrum from quiet solar radio emission, the pre-burst background level (right panels of Figure 1) is always subtracted from the radio bursting image.

When the Sun is near the horizontal, the interference between the antenna direction and the ground-reflected ray from the Sun may produce spurious structure in the spectra of some types of bursts, e.g., Type II. This is called ‘Lloyd’s Mirror’ effect. At high frequency, the ground reflections are negligible because the parabolic reflector antennas (IRS-2 and IRS-3) have narrower beams and low side lobes. However the effects can’t be negligible where the LPA (IRS-1) with broad beam is used (Nelson *et al.*, 1985). For this reason, the interpretation of type II burst structure should be done with great caution at sunrise and sunset. The use of harmonic bursts for the accurate estimation of coronal shock speeds would be the most suitable to minimize the error due to ground reflections, since these bursts usually start at a higher frequency than the fundamental. Thus we have used the harmonic bursts to estimate the drift rates for the most events, especially when the Sun is near the horizon.

3. Results

We have observed 34 type II bursts in the range 30 - 2500 MHz during the time period May 1998 - November 2000. By employing the Newkirk (1961) model to maintain consistency with other observatories, coronal shock speeds are estimated from the drift rates of type II bursts. Table II shows the details of 34 type II bursts observed using our spectrograph together with those of associated GOES soft X-ray (1-8Å) flares from National Geophysical Data Center (NGDC; <ftp://ftp.ngdc.noaa.gov>) and associated CMEs from a SOHO/LASCO CME Catalog of CSPSW/NRL (Yashiro and Michalek, 2002). The first 4 columns give the event number, date, time, and shock speed determined by type II bursts. The fifth column lists other observatories that observed the events. The next 6 columns provide the flare and CME information; the ΔT ’s in the latter 4 columns will be defined and discussed below.

All the type II bursts detected by our spectrograph were simultaneously observed by other observatories as shown in Table II, column 5. Our estimated shock speeds are compared with those from other observatories including Culgoora, Hiraiso, and Learmonth RSTN site. Their estimated shock speed data are available in the NGDC website (ftp://ftp.ngdc.noaa.gov/STP/SOLAR_DATA/SOLAR_RADIO/SPECTRAL/). Figure 2 shows that our speeds are similar to those of

Table II. Details of the solar type II bursts observed by RRL spectrograph.

Event		Type II			X-ray Flare				CME	
No.	Date	Time (UT)	Speed ^a (km s ⁻¹)	Obs. ^b Sites	Location (degree)	Mag.	ΔT_{XII} ^c (min)	$\Delta T_{X'II}$ ^d (min)	ΔT_{CII} ^e (min)	$\Delta T_{C'II}$ ^f (min)
1	08 May 1998	02:00-02:06	SH569	C, H, L	S15W85	M3.1	-11	4	-16.8	-17.0
2	08 May 1998	06:01-06:03	FN1100	C, H	S15W85	M1.4	-8	7	-3.4	-12.9
3	29 May 1998	00:58-01:10	SH500	C, H, L	N18W94	M6.7	-7	1	-17.4	-16.4
4	30 May 1998	22:48-22:51	SH737	C, H	-	-	-	-	-9.8	-21.0
5	31 July 1998	05:33-05:44	SH650	C	N28E31	C2.9	-8	5	-	-
6	26 May 1999	02:36-02:39	FN700	C, H	N22E41	C2.3	-11	-6	-	-
7	29 May 1999	03:11-03:23	SH612	C	S20E80	M1.6	-7	4	-9.6	-9.5
8	11 June 1999	00:39-00:41	SH1150	C	-	-	-	-	0.9	-12.4
9	11 June 1999	00:50-00:56	SH546	C	-	-	-	-	-	-
10	23 June 1999	05:45-05:52	SH1083	C, H	-	-	-	-	-15.7	-23.2
11	11 July 1999	00:14-00:16	SH772	C	N18E32	C3.0	-5	5	7.9	-18.2
12	11 July 1999	00:21-00:26	SH530	C	N18E32	C3.0	-12	-2	-	-
13	13 July 1999	06:02-06:04	FN874	C, H	N16E06	C2.9	-40	-16	-	-
14	04 Aug. 1999	05:51-05:57	SH1027	H	S16W64	M6.0	-6	5	-0.8	-0.7
15	17 Aug. 1999	04:53-04:56	SH422	C, H	-	-	-	-	-4.7	-6.9
16	20 Aug. 1999	23:21-23:25	SH474	L	S25E64	M9.8	-18	-13	-28.6	-36.9
17	27 Oct. 1999	04:31-04:33	SH1118	C, H, L	N08E34	C5.3	-5	-1	-	-
18	12 Feb. 2000	04:04-04:06	SH778	C, H, L	N26W23	M1.7	-13	6	5.1	3.8
19	12 Feb. 2000	04:12-04:15	FN793	C, H	N26W23	M1.7	-21	-2	-	-
20	02 Mar. 2000	08:27-08:31	FN1321	H	S14W52	X1.1	-7	1	-15.6	-15.2

Table II. (continued)

Event		Type II			X-ray Flare				CME	
No.	Date	Time (UT)	Speed ^a (km s ⁻¹)	Obs. ^b Sites	Location (degree)	Mag.	ΔT_{XII} ^c (min)	$\Delta T_{X'II}$ ^d (min)	ΔT_{CII} ^e (min)	$\Delta T_{C'II}$ ^f (min)
21	24 Mar. 2000	07:51-07:57	SH617	C, H, L	N16W82	X1.8	-10	1	–	–
22	25 Mar. 2000	22:35-22:45	SH650	C, H, L	S14W02	C7.4	-4	8	14.1	10.1
23	27 Mar. 2000	06:46-06:52	SH1330	C, H, L	S17E42	C2.3	-9	8	-27.2	-53.9
24	27 Mar. 2000	06:54-07:01	SH364	C	S17E42	C2.3	-17	0	–	–
25	06 Apr. 2000	02:27-02:32	SH1000	C, H, L	S15E53	M1.8	-9	2	-12.4	-14.4
26	09 Apr. 2000	23:38-23:43	FN760	C, H, L	S14W01	M3.1	-12	4	–	–
27	20 May 2000	05:55-05:59	SH565	C, H, L	S15W08	C7.6	-30	-20	-35.6	-37.5
28	05 June 2000	03:21-03:25	SH560	C, H, L	S11W32	C4.5	-9	4	4.52	0.11
29	10 July 2000	21:23-21:27	SH1229	C	N18E49	M5.7	-18	19	–	–
30	25 July 2000	02:48-02:52	FN934	C, L	N06W08	M8.0	-5	1	0.5	-2.8
31	09 Oct. 2000	23:39-23:43	SH1100	C, L	N01W14	C6.7	-20	4	-27.1	-31.6
32	09 Oct. 2000	23:43-23:52	SH743	C	N01W14	C6.7	-24	0	–	–
33	24 Nov. 2000	05:04-05:08	SH1167	C, L	N23W05	X2.0	-9	-2	4.9	2.4
34	29 Nov. 2000	06:29-06:44	SH480	C	S13E43	C9.1	-10	0	–	–

^a SH denotes second harmonic component of type II burst and FN, Fundamental component.

^b Observatories which observed the same event, C: Culgoora, H: Hiraiso, L: Learmonth.

^c Time difference between X-ray start and type II burst start.

^d Time difference between X-ray peak and type II burst start.

^e Time difference between CME start with extrapolated acceleration back to $1.1R_{\odot}$ and type II burst start. The dash(–) indicates that no CME was observed.

^f Time difference between CME start with extrapolated constant speed back to $1.1R_{\odot}$ and type II burst start.

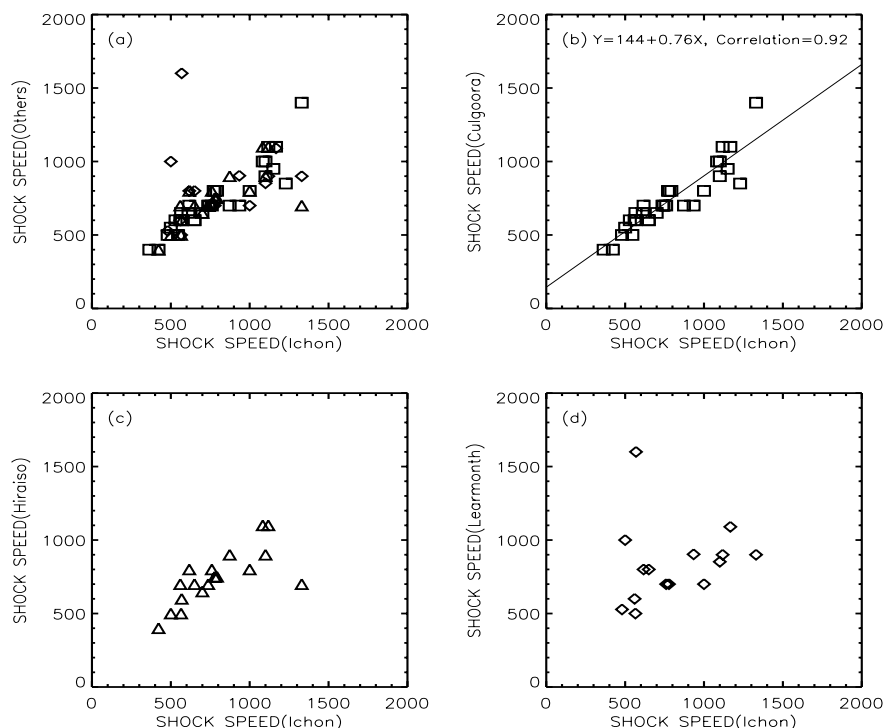


Figure 2. Estimated shock speeds from IRS compared with those of other observatories: all observatories(a), Culgoora(b), Hiraiso(c), and Learmonth(d).

other observatories and have a good linear correlation with those from the Culgoora observatory ($r=0.92$). The several discrepancies between our speeds and the other observatories are possibly due to subjective choices in choosing specific frequency-time points on the spectrogram.

We have examined the association of type II burst data with solar flares and CMEs according to time closeness. Of these 34 events, only 5 events did not appear to be associated flares identified by GOES X-ray data; these could be behind-the-limb events (events 4, 8, 9, 10, and 15). In addition we identified 21 events, which are likely to be related to CMEs. For the comparison of these type II bursts with associated X-ray flares and CMEs, the latter onset times are extrapolated back to $1.1 R_{\odot}$ by using either a constant CME speed from a linear fit or a speed and an acceleration from a quadratic fit, in the data of SOHO/LASCO CME catalog by Yashiro and Michalek (2002). The locational information of flares and their GOES X-ray times were obtained from NGDC. We have examined the time differences between start of the type II burst and start, as well as the peak, of X-ray intensity. We also extrapolated

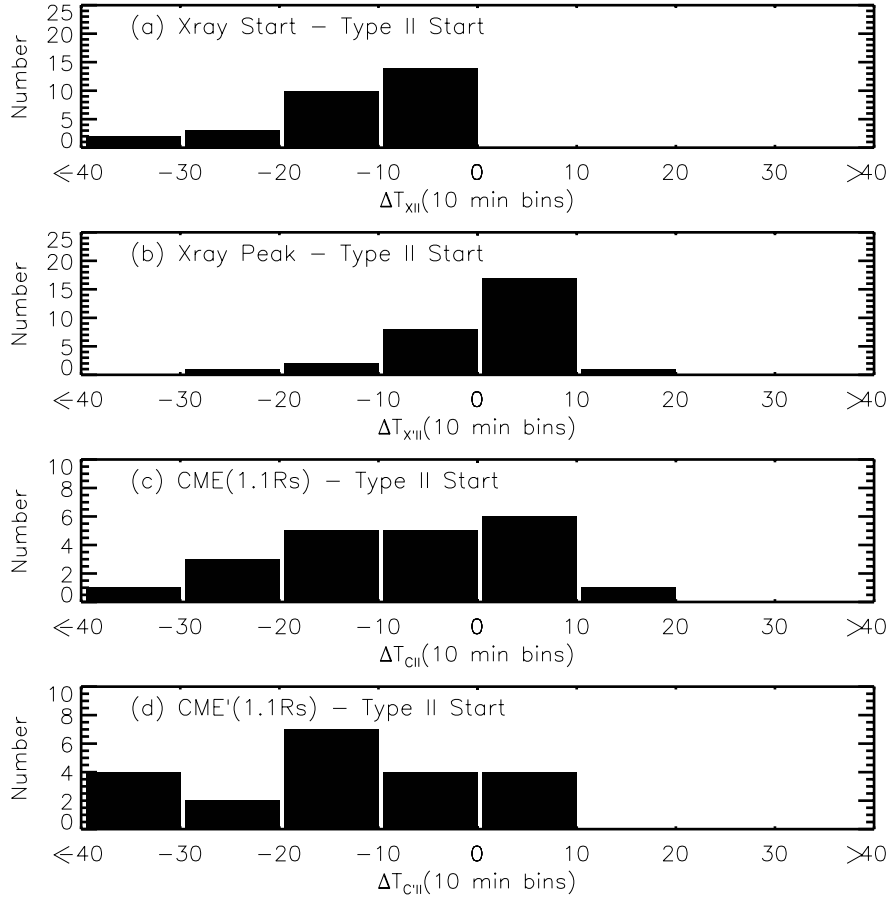


Figure 3. Comparison of start times of type II bursts detected by IRS, CME onset time extrapolated, GOES X-ray flare start, and GOES X-ray flare peak time: (a) time difference between X-ray start and type II burst start using 10 minute bins, (b) time difference between X-ray peak and type II burst start, (c) time difference between the CME onset time extrapolated at $1.1R_{\odot}$ by using CME acceleration and speed, and type II burst start, and (d) time difference between the CME onset time extrapolated at $1.1R_{\odot}$ by using constant speed CME, and type II burst start.

CME onset time to show how these events were correlated in time. The results (Figure 3) are:

- (1) All the identified type II bursts start after the onset of the X-ray flares (a);
- (2) Most of the type II bursts start within 10 min before and after X-ray peak time (b); and
- (3) Most of the CME onset times at $1.1 R_{\odot}$ are earlier than start of the type II bursts for both cases (c) and (d).

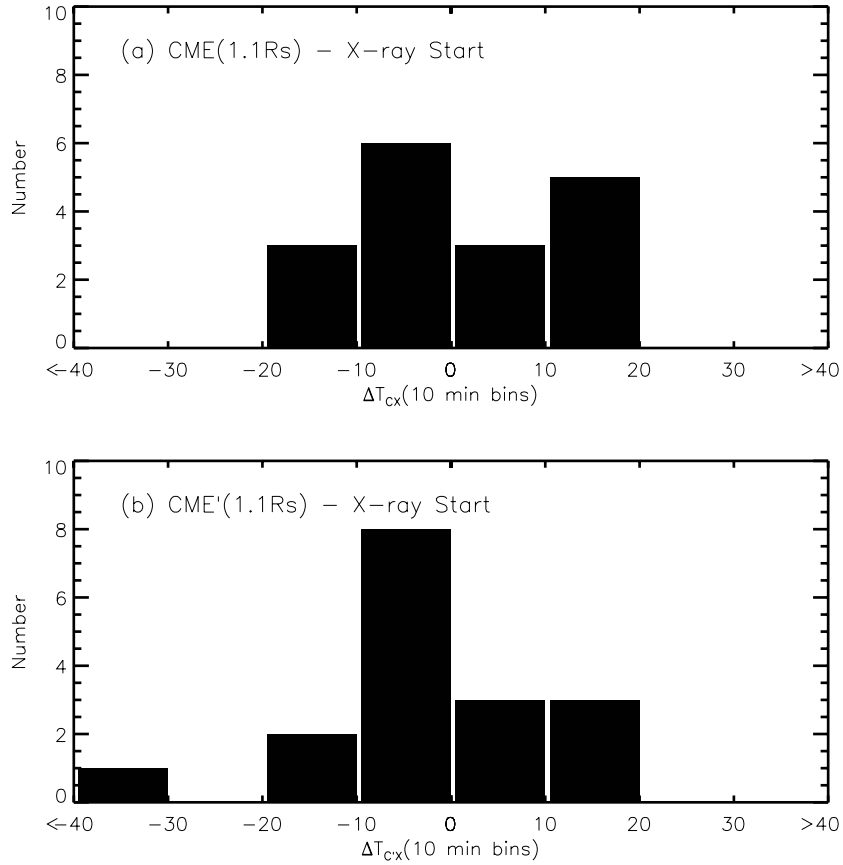


Figure 4. Comparison of the CME onset time extrapolated at $1.1R_{\odot}$ and GOES X-ray flare start time using two different extrapolation methods: (a) by CME speeds and accelerations and (b) by CME constant speeds.

From two results shown in Figure 3-(a) and 3-(b), one can reasonably assume that the shock has developed during the rise time of the physical process that generates the X-ray emission. As noted in the legend for Figure 3, the C'II in the ΔT subscript refers to the CMEs' constant speed extrapolation for the calculation of the time difference: (CME' ($1.1 R_{\odot}$) minus the type II start time). As seen in Figures 3-(c) and 3-(d), the onset time differences between type II bursts and CMEs are a little smaller in the case (Figure 3-(c)) where we consider both speed and acceleration data for the extrapolation of CME onset time. It is important to point to some restrictions on the question of CME onset vis-a-vis the type II start time. The actual height of the CME start can be anywhere above, at (as assumed here) or below $1.1 R_{\odot}$.

Examination of CME speeds in the plane-of-sky is a highly subjective topic that depends on the choice of position angle for, presumably, the fastest part of the white-light intensity increase above background. The CME's leading edge is often irregular and far from being a smooth circular arc. Also, little is known about the motion out-of-the-plane-of-sky. Subjectivity in the choice of position angle for the CME's 'leading edge' is again an important uncertainty. This is true especially in the extrapolation of the observed points down below the SOHO/LASCO C2's occulting disk at $2 R_{\odot}$.

Figure 4 shows a comparison of the CME onset time extrapolated at $1.1 R_{\odot}$ and GOES X-ray flare start time using two different extrapolation methods: by constant speeds and by speeds based on second order acceleration fits. For both methods, all of the onset time differences except for one event between CMEs and flares fall within ± 20 min. This implies that CMEs and flares are initiated at nearly the same time. In this sense, it is interesting to note that Zhang *et al.* (2001) and Neupert *et al.* (2001) analyzed in detail the initial eruptions of CMEs using the EUV imaging telescope and the LASCO C1 coronagraph (with field of view 1.1 to $3.0 R_{\odot}$) on board SOHO and showed that CME accelerations coincided with the rapid increases of GOES X-ray fluxes.

4. Summary and Discussion

In this paper we have introduced a new solar radio spectrograph recently installed at Ichon branch of Radio Research Laboratory, Korea. Daily observation is performed nearly automatically from data acquisition to processing. A minimum smoothing method is successfully applied to improve the quality of observation. As a result, we have successfully observed typical solar radio bursts.

As first results we have presented 34 metric type II bursts during the time period May 1998 - November 2000. Coronal shock speeds were estimated from the drift rates of 34 type II bursts. It is shown that our speeds are similar to those of other observatories. We are making a data analysis software to estimate the coronal shock speeds in near-real time. Then it is expected that our type II burst data will soon be used for space weather prediction tools such as 'fearless forecasting' real time shock arrival predictions (Fry *et al.*, 2001, 2002, and their real time website, <http://www.expi.net/expinet/tools.html>).

We have also found that most of the observed type II bursts (29/34) appear to be associated with X-ray/optical flares, and 21 type II bursts have CMEs with near-simultaneous time coincidence. Type II burst

onset times were also compared with the start/peak times of X-ray intensity and the extrapolated onset times of CMEs. From the time comparison, we have found the following facts: (1) all the identified type II bursts start after the onset of the X-ray flares; and (2) most of the type II bursts start within 10 min before and after X-ray peak time.

We have also compared the CME onset time extrapolated at $1.1R_{\odot}$ with GOES X-ray flare start time using two different extrapolation methods: constant speed and acceleration. For both cases, we have found that the onset time differences between CMEs and flares fall within ± 20 min. In this sense, it is interesting to note that, even though there are some uncertainties in the CME onset time measurements, our results support the idea that CMEs and flares initiated near-simultaneously, at least for type II associated events. This fact is consistent with recent results of Zhang *et al.* (2001) and Neupert *et al.* (2001) who showed that CME accelerations coincided with the rapid rises of GOES X-ray fluxes from the initial eruption studies of CMEs.

Acknowledgements

We thank Drs G. Michalek and S. Yashiro very much for their help to identify the first C2 appearance times and heights of CMEs. We are also thankful to the referee for his/her valuable comments, which helped us improve the paper. KSC thanks Drs R. Thompson (IPS/Radio and Space Services), M. Akioka (CRL/Hiraiso Solar Observatory), T. Kondo (CRL/Kashima Space Research Center) and C. D. Fry (Exploration Physics International) for their constructive suggestions. KSK appreciates the support of Korea Astronomy Observatory. YJM acknowledges the support of MURI grant of AFOSR and National Research Laboratory grant M10104000 059-01J000002500 of the Korean government. MD acknowledges the support of the Geophysical Institute (University of Alaska at Fairbanks) under the DoD project, University Partnering for Operational Support (UPOS), as well as the hospitality of the NOAA Space Environment Center.

References

- Cho, K. S., Lee, G. H., and Kim, K.-S.: 1997, *J. Astron. Space Sci.* **14**, 320 (in Korean).
Cliver, E. W., Webb, D. F., and Howard, R. A.: 1999, *Solar Phys.* **187**, 89.
Dryer, M.: 1994, *Space Sci. Rev.* **67**, 363.
Dryer, M.: 1996, *Solar Phys.* **169**, 421.

- Dryer, M. and Smart, D. F.: 1984, *Adv. Space Res.* **4**, 291.
- Fry, C. D. *et al.*: 2001, *J. Geophys. Res.* **106**, 20985.
- Fry, C. D., Sun, W., Deehr, C. S., Dryer, M., Smith, Z., and Akasofu, S.-I.: 2002, *Adv. Space Res.*, in press.
- Gopalswamy, N. *et al.*: 1998, *J. Geophys. Res.* **103**, 307.
- Gopalswamy, N., Kaiser, M. L., Sato, J., and Pick, M.: 2000, in R. Ramaty and N. Mandzhavidze (eds.), *Publ. Astron. Soc. Pac. Conf. Ser.* **206**, 351.
- Gosling, J. T.: 1993, *J. Geophys. Res.* **98**, 18937.
- Gosling, J. T. and Hundhausen, A. J.: 1995, *Solar Phys.* **160**, 57.
- Klassen, A., Aurass, H., Mann, G., and Thompson, B. J.: 2000, *Astron. Astrophys. Suppl. Ser.* **141**, 357.
- Kondo, T., Isobe, T., Watari, S., and Tokumaru, M.: 1995, *J. Commun. Res. Lab.* **42**, 111.
- Krüger, A.: 1979, *Introduction to Solar Radioastronomy and Radio Physics*, D. Reidel Publ. Co., Dordrecht, Holland.
- Leblanc, Y., Dulk, G. A., Vourlidas, A., and Bougeret, J.-L.: 2001, *J. Geophys. Res.* **106**, 25301.
- Mann, G., Aurass, H., Voigt, W., and Paschke, J.: 1992, *Proceedings of the First SOHO Workshop*, Maryland, ESA SP-348, 129.
- Mann, G. *et al.*: 1996, *Astron. Astrophys. Suppl. Ser.* **119**, 489.
- Messmer, P., Benz, A. O., and Monstein, C.: 1999, *Solar Phys.* **187**, 335.
- Nelson, G. J., Sheridan, K. V., and Suzuki, S.: 1985, in D. J. McLean and N. R. Labrum (eds.), *Solar Radiophysics*, Cambridge University Press, Cambridge, p. 113.
- Neupert, W. M., Thompson, B. J., Gurman, J. B., and Plunkett, S. P.: 2001, *J. Geophys. Res.* **106**, 25215.
- Newkirk, G. Jr.: 1961, *Astrophys. J.* **133**, 983.
- Prestage, N. P., Luckhurst, R. G., Paterson, B. R., Bevins, C. S., and Yuile, C. G.: 1994, *Solar Phys.* **150**, 393.
- Reiner, M. J. *et al.*: 2001, *J. Geophys. Res.* **106**, 25279.
- Robinson, R. D.: 1985, *Solar Phys.* **95**, 343.
- Shanmugaraju, A., Umopathy, S., Balasubramanian, V., Selvanayagam, A. J., and Manoharan, P. K.: 1999, *Solar Phys.* **188**, 155.
- Smart, D. F. and Shea, M. A.: 1985, *J. Geophys. Res.* **90**, 183.
- Smerd, S. F., Sheridan, K. V., and Stewart, R. T.: 1975, *Astrophys. Lett.* **16**, 23.
- Smith, Z. and Dryer, M.: 1990, *Solar Phys.* **129**, 387.
- Svestka, Z.: 1995, *Solar Phys.* **160**, 53.
- Thompson, R., Kennewell, J., and Prestage, N.: 1996, *Solar Phys.* **166**, 371.
- Thompson, B. J. *et al.*: 2000, *Astrophys. J.* **517**, L151.
- Vrsnak, B., Ruzdjak, V., Zlobec, P., and Aurass, H.: 1995, *Solar Phys.* **158**, 331.
- Wagner, W. J. and McQueen, R. M. : 1983, *Astron. Astrophys.* **120**, 136.
- Wild, J. P. and McCready, L. L.: 1950, *Australian J. Sci. Res.* **3**, 387.
- Yashiro, S. and Michalek, G.: 2002, <http://cdaw.gsfc.nasa.gov/CME.list/>.
- Zhang, J., Dere, K. P., Howard, R. A., Kundu, M. R., and White, S. M.: 2001, *Astrophys. J.* **559**, 452.